ELSEVIER

Journal of Hydrology 158 (1994) 1–18

Journal of Hydrology

[1]

Runoff model sensitivity to radar rainfall resolution

Fred L. Ogden*,[a], Pierre Y. Julien[b]

[a]*Iowa Institute of Hydraulic Research, University of Iowa, Iowa City, IA 52242, USA*
[b]*Department of Civil Engineering, Colorado State University, Fort Collins, CO 80523, USA*

(Received 27 January 1993; revision accepted 16 January 1994)

Abstract

Rainfall rates estimated from polarimetric weather radar measurements of a convective rainstorm are used as input to a two-dimensional physically based rainfall–runoff model. The correlation length of the input rainfall field L_S is 2.3 km. Runoff simulations are performed on two semi-arid watersheds covering 32 km^2 and 121 km^2 at basin data grid sizes L_M of 125 m and 200 m, respectively. The characteristic basin length scale L_W is taken as the square root of the watershed area. Rainfall data at resolutions L_R of 1, 2, 3, 4, 6 and 8 km serve as model input to determine the effect of precipitation data spatial resolution on computed outflow hydrographs. Two dimensionless length parameters are identified which describe the similarity of the effect of rainfall data aggregation on both basins. The first parameter, L_R/L_S, describes 'storm smearing', and the second parameter, L_R/L_W, describes 'watershed smearing'. Results from simulations without infiltration show storm smearing occurring as $L_R \rightarrow L_S$. Watershed smearing causes more significant deviations from simulations using the finest-resolution data when L_R/L_W exceeds 0.4. Results with infiltration reveal that excess rainfall volumes decrease with increasing L_R/L_W. Additionally, excess rainfall volumes do not converge as L_R/L_W is decreased to the practical lower limit provided by contemporary weather radars, which is of the order of 1 km.

1. Introduction

The NEXRAD weather radar network being installed in the USA will provide quantitative digital estimates of the spatial distribution of rainfall. Approximately 160 NEXRAD WSR-88D radars are being deployed throughout the USA and at selected overseas sites (Klazura and Imy, 1993). The radar network will observe approximately 95% of the 48 conterminous USA at beam heights less than 3000 m

* Corresponding author (formerly at Colorado State University).

SSDI 0022-1694(94)02462-K

List of Symbols

A	Area of watershed (L^2)
K_{DP}	Specific differential propagation phase shift (deg L^{-1})
L_M	Runoff model raster grid size (L)
L_R	Precipitation data grid size (L)
L_S	Rainfall correlation length (L)
L_W	Watershed characteristic length ($= A^{1/2}$) (L)
M_d	Soil moisture deficit
n	Manning roughness coefficient ($L^{1/3}T$)
Q_p	Peak total flow rate ($L^3 t^{-1}$)
$\bar{Q}_p$	Mean normalized peak total flow rate
Q_p^*	Normalized peak total flow rate
R	Rainfall rate (LT^{-1})
S_{Q_p}	Standard deviation of normalized peak outflow
S_{V_o}	Standard deviation of normalized outflow volume
S_{V_r}	Standard deviation of normalized rainfall volume
V_o	Volume of outflow (L^3)
$\bar{V}_o$	Mean normalized outflow volume
V_o^*	Normalized outflow volume
V_r	Volume of rainfall (L^3)
$\bar{V}_r$	Mean normalized rainfall volume
V_r^*	Normalized rainfall volume
Z_{DR}	Differential reflectivity
Z_H	Radar reflectivity factor ($L^6 L^{-3}$)
Greek letters	
ϕ_{DP}	Differential propagation phase shift (deg)

above ground level. NEXRAD radars record the spatial distribution of the radar reflectivity factor Z at resolutions ranging from 1 to 4 km, at 15 min temporal resolution. The full hydrologic application of these data requires hydrologic models capable of accepting spatially distributed rainfall. Models of this type, referred to as 'distributed' hydrologic models, are typically physically based and operate on sub-catchments or raster elements which are considerably smaller than the watershed under study.

Given the tremendous quantity of data collected by each NEXRAD site over the course of a year, there is a need to determine if the data may be aggregated and still retain usefulness for hydrologic modeling (National Research Council, 1991, p. 267). Temporal and spatial aggregation tend to reduce rainfall gradients. Physically based rainfall–runoff models are sensitive to the rainfall rate, particularly in determining excess rainfall. The purpose of this study is to examine the sensitivity of a physically based distributed watershed rainfall–runoff model to the spatial resolution of radar rainfall input data. The results of this study have implications for the use of radar-estimated rainfall in real-time flood forecasting, physically based flood frequency analysis using historical radar data, and issues of scale in the rainfall–runoff modeling process.

2. Review of literature

Several recent studies have addressed the issue of remotely sensed precipitation data resolution for watershed modeling. Kouwen and Garland (1989) examined the effect of changing radar rainfall data spatial resolution on a one-dimensional composite square grid distributed parameter watershed model. A 3250 km^2 watershed was simulated using the SIMPLE (Kouwen, 1986) watershed model, with rainfall data grid sizes of 2 km × 2 km and 10 km × 10 km. A total of 30–50 precipitation input grid cells over the watershed were found to model the precipitation field adequately for flood forecasting purposes. A maximum radar resolution of 10 km × 10 km was sufficient for modeling floods produced by either thunderstorms or frontal systems.

Ogden and Turk (1991) examined the effect of radar resolution on the runoff from the 32.2 km^2 Macks Creek, Idaho, watershed using a two-dimensional surface runoff model. Single-parameter (Z) radar data from one storm were gridded at 152 m resolution with a reflectivity–rainfall (Z–R) relationship and applied at successively coarser resolutions. From simulations with only one storm the following conclusions were reached: as the radar grid size was coarsened from 152 m to 5 km, the magnitudes of the peak outflow and outflow volume decreased, whereas the time to peak increased. Hail contamination of the reflectivity signal was noted as a source of unrealistically high rainfall rates.

A Monte Carlo technique was used to study the effect of rain-gauge sampling resolution on a distributed watershed model by Krajewski et al. (1991). The distributed model consisted of a series of one-dimensional distributed stream tube subcatchments, and was based on the kinematic wave overland flow approximation. The findings of this study indicate that model response is more sensitive to temporal resolution than spatial resolution of the input precipitation data. The performance of the distributed model was compared with that of a lumped model. The results indicated that lumped parameter models consistently underestimate peak flows. Krajewski et al. concluded that a two-dimensional square grid model would be better suited to modeling the problem of optimal spatial and temporal resolution.

Dual polarization radar data (Z_H, Z_{DR}) were applied with a linear runoff model by Seliga et al. (1991) to examine the model sensitivity to temporal and spatial variation in precipitation intensity. The runoff model combined elements of unit hydrograph theory and Soil Conservation Service (SCS) curve number analysis. The resolution of the input data, reflected by the size and number of model hydrologic response units (HRUs), was also examined for effect on the runoff model. The results indicated that the watershed response was greatly influenced by the available spatial resolution of the precipitation data, as well as the size of the HRUs used in the model. Seliga et al. concluded that an HRU size of approximately 5 km^2 is adequate. Additionally, the findings indicate that as the HRU size is decreased the magnitudes of the peak outflows do not converge.

The value of weather radar in flood forecasting was examined by Pessoa et al. (1993), in a sensitivity analysis of the distributed basin simulation (DBS) distributed hydrologic model (Cabral et al., 1990) of the 840 km^2 Sieve River basin in Italy. Weather radar data from the MIT C-band radar was transposed and applied to the

Sieve model. The parameters varied include radar data temporal and spatial resolution, the $Z-R$ relationship, and radar signal quantization. The model was found to be most sensitive to the spatial resolution of the radar data, and relatively insensitive to the temporal resolution and data quantization.

Physically based rainfall–runoff model sensitivity to rainfall temporal and spatial variability was examined by Ogden and Julien (1993). The sensitivity of impervious watersheds to the spatial variability of rainfall decreases, inversely with time, to a small value after equilibrium conditions are reached. The opposite is true for rainfall temporal variability, as the sensitivity increases toward an asymptotic value after the time to equilibrium.

3. Objectives

This paper provides a basis for the discussion of radar data spatial resolution requirements for physically based hydrologic modeling of small basins covering less than 150 km^2. The specific objectives of this study are the following: (1) to analyze rainfall data spatial resolution, in the context of length scales, to identify dimensionless similarity parameters which describe conditions where rainfall grid size affects the response of surface runoff models; (2) to examine impervious runoff simulations to determine the effects of precipitation data spatial resolution on peak discharge and rainfall–runoff volumes in terms of dimensionless similarity parameters; (3) to examine runoff simulations of pervious basins to determine the effect of precipitation data resolution on the magnitude of the computed peak discharge, and runoff model sensitivity to rainfall data grid size for various degrees of initial soil saturation.

4. Study watersheds and surface runoff model

The CASC2D (Julien and Saghafian, 1991) watershed rainfall–runoff model was used in this study. CASC2D is a two-dimensional, raster-based, distributed hydrologic model. Overland flow routing is based on a two-dimensional explicit solution of the diffusive wave form of the de St. Venant equations, with friction slopes calculated by the Manning equation. Surface slopes are calculated from digital elevation model (DEM) data. Overland flow is routed in two orthogonal directions within each raster grid element. Channel routing is performed by an explicit diffusive wave formulation.

The three-parameter Green and Ampt (1911) method is used in CASC2D to calculate infiltration rates. The three Green and Ampt parameters (hydraulic conductivity at natural saturation, capillary pressure head at the wetting front, and the soil moisture deficit) can be measured in the field. The head of water on the soil surface was neglected as being much smaller than the capillary pressure head. Soil characteristic data, in the form of SCS textural classifications, were used to define the infiltration parameters of the soils on both Macks Creek and Taylor Arroyo, using the data of Rawls et al. (1983). There are provisions within the model to account for interception and detention storage.

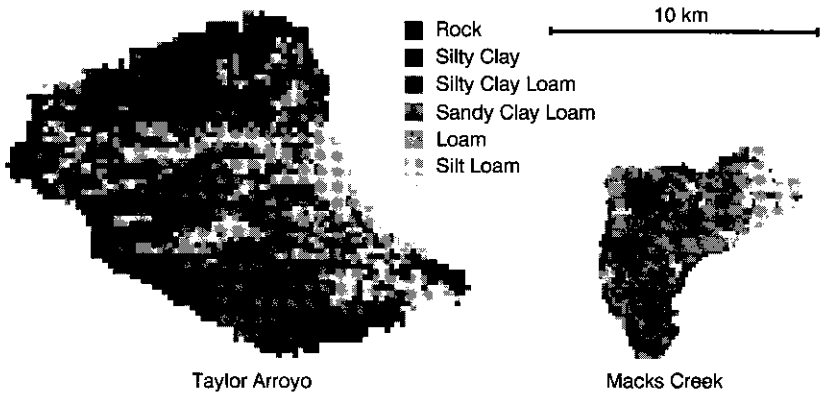

Fig. 1. Soil type maps for Macks Creek and Taylor Arroyo (to scale).

The two semi-arid watersheds selected for this study are the 32 km^2 Macks Creek watershed in southwestern Idaho, and the 121 km^2 Taylor Arroyo watershed in southeastern Colorado. Macks Creek has an average slope of 9.4%, with slopes in some regions in excess of 30%. Macks Creek is an ephemeral stream with flashy response to intense rainstorms. The larger Taylor Arroyo watershed is moderately pervious and has an average slope of 1.6%. Both watersheds can be appropriately modeled using Hortonian runoff production mechanisms. The Macks Creek and Taylor Arroyo elevation data were input to CASC2D at resolutions L_M of 125 m and 200 m, respectively. A watershed characteristic length L_W is taken as the square root of the watershed area. The L_W values for Macks Creek and Taylor Arroyo are 5.7 km and 11.0 km, respectively. The calibration of CASC2D on Macks Creek was performed by Saghafian (1992), and on Taylor Arroyo by Doe (1992). The spatially distributed soil types on Macks Creek and Taylor Arroyo are shown to scale in Fig. 1. The corresponding Green and Ampt soil parameter values are listed in Table 1.

The starting conditions used in all impervious simulations were identical: no surface water, and a constant value of Mannings n of 0.04 over the entire watershed. In simulations with infiltration, the initial soil moisture deficit was varied, and all other soil and basin characteristics remained unchanged. For each

Table 1
Green and Ampt soil parameter values for the soil texture classes shown in Fig. 1

Soil texture class	Total porosity ($cm^3\,cm^{-3}$)	Effective porosity ($cm^3\,cm^{-3}$)	Wetting front capillary pressure (cm)	Hydraulic conductivity ($cm\,h^{-1}$)
Silt loam	0.501	0.486	16.68	0.65
Loam	0.463	0.434	8.89	0.34
Sandy clay loam	0.398	0.330	21.85	0.15
Silty clay loam	0.471	0.432	27.30	0.10
Silty clay	0.479	0.423	29.22	0.05
Rock	–	–	–	0.00

simulation the entire outflow hydrograph was saved in an output file, with the time to peak, peak discharge, total outflow volume, and total rainfall volume in a separate summary file.

5. Advances in radar rainfall estimates

This study required a high-quality spatially distributed rainfall data set. Recent polarimetric weather radar techniques offer an opportunity to record spatially distributed rainfall data with unprecedented accuracy. The weather radar data used in this study were recorded by the CSU-CHILL radar facility, which is located near Greeley, Colorado, and jointly funded by Colorado State University and the National Science Foundation. The radar is a dual linearly polarized coherent radar which operates at 2.750 GHz, corresponding to a wavelength of 10.7 cm in the S band. The beamwidth of the 8 m diameter antenna is approximately 1.0°. Attenuation does not affect S-band weather radars, even in the heaviest rainfall, making them ideal for weather observation. The radar transmits an average power of 1 kW with peak power during transmit pulses of 1 MW, and can measure Doppler velocities.

The dual polarization capabilities of the CSU-CHILL radar allow observation of precipitation in two orthogonal polarization states. The recorded radar observables include the reflectivity factor in horizontal polarization Z_H, the differential reflectivity Z_{DR} (Seliga and Bringi, 1976), and the differential propagation phase ϕ_{DP} (Sachidananda and Zrnic, 1986). The reflectivity factor, Z_H, is an integrated measure of the sixth power of the raindrop size distribution (RSD) over the entire pulse volume. The rainfall rate may be estimated from Z_H by assuming the form and parameters of the RSD and a raindrop fall speed relationship. Such Z–R relationships are often empirically derived. One shortcoming of the use of the reflectivity factor in rain rate estimation is the heavy weighting of the largest particles in the radar pulse volume. Wet hail, for instance, can completely dominate the return signal and mask any useful information from liquid-phase hydrometeors.

Dual linearly polarized radars measure the reflectivity factor in two orthogonal (horizontal and vertical) polarizations, Z_H and Z_V. Differential reflectivity, Z_{DR}, arises because raindrops tend to flatten in their vertical dimension as they grow and fall. The differential reflectivity is given by $Z_{DR} = Z_H - Z_V$, providing an indirect indicator of raindrop oblateness, and therefore size. Using an assumed RSD, Z_{DR} will provide an estimate of one of the RSD parameters. When combined in a relationship with Z_H, a more accurate estimate of the rainfall rate may be obtained. Another appealing aspect of Z_{DR} is in hail identification. Hail particles tend to be nearly spherical, and tumble as they fall. Therefore, the differential reflectivity will tend to be near zero in high-reflectivity regions with hail present, and large if no hail is present. However, if hail is present within a pulse volume, rain rate relationships based on either Z_H or Z_{DR} cannot be used to estimate the rainfall rate (Jameson, 1991), and another method must be applied.

The refractive indices of the atmosphere and of liquid- and ice-phase hydrometeors

are different. As the electromagnetic radiation emitted by the radar passes through a hydrometeor, its speed is changed. Therefore, upon emergence from the hydrometeor, its phase will be lagged somewhat relative to radiation which did not pass through it. As liquid hydrometeors tend to flatten as they become larger, there is a difference between the phase shift of radiation at horizontal and vertical polarization. This differential phase shift, ϕ_{DP}, is an integrated measure of the quantity of liquid water over the entire propagation path, that is, from radar to target and back to the radar. The specific differential propagation phase, K_{DP}, is defined as one-half the spatial derivative of ϕ_{DP}. The parameter K_{DP} is useful in hydrometeorology because it is insensitive to hail, independent of the reflectivity factor, and nearly linearly proportional to the rainfall rate (Sachidananda and Zrnic, 1986).

The expected accuracy of rainfall rates determined using polarimetric techniques was examined by Chandrasekar et al. (1993). In simulations without hail, it was found that the fractional standard deviation (FSD) of rainfall rate estimated from Z_H is approximately 45% for rain rates less than 10 mm h^{-1}, increasing to 55% at 150 mm h^{-1}. The FSD of rain rate estimated with Z_H and Z_{DR} was 60% for rain rates less than 10 mm h^{-1}, and approximately 25% for higher rain rates. Using K_{DP} as the sole rain rate estimator, the FSD was observed to decrease from approximately 80% at 20 mm h^{-1} to 25% at 80 mm h^{-1} and 15% at 200 mm h^{-1}.

The radar data used in this study were recorded on 3 June 1991, and covered the entire lifetime of a convective squall line between 12 and 60 km from the radar. The storm began at approximately 12:00 h MDT. Surface heating and local instability initiated convective activity. The uplifting air created a convergence line along which the most intense thunderstorm cells were located. Data were recorded for 2 h 15 min at 5 min increments. The radar was operated in a volume scan mode, with four elevation angles per volume scan. There was significant beam blockage at the lowest elevation angle scan (0.5°), so the next highest elevation angle (1.6°) was used to estimate the rainfall rates. Ground observers noted large quantities of pea-size hail from this storm.

The following polarimetric algorithm was used to estimate the rainfall rates. In high-reflectivity regions $Z_H > 40$ dBZ, the K_{DP} relationship of Chandrasekar et al. (1990) was used to estimate the rainfall rate. In all other instances, the combined Z_H and Z_{DR} relationship of Chandrasekar et al. (1990) was used, unless $Z_{DR} < 0$. In such cases, rainfall was estimated with Z_H via the Austin (1987) Z–R relationship.

The rainfall fields were converted from radar conical coordinates to rectangular coordinates by interpolation to 1 km × 1 km grid size. Figs. 2 and 3 show multi-parameter estimated rainfall rates within the 80 km × 80 km square data domain, at 12:48 h MDT and 13:56 h MDT, respectively. The radar is located at the origin of the plots. The scale of individual storm cells is approximately 4 km–10 km, with an average value near 8 km. The rainfall data from the 27 radar scans were processed to determine the correlation length. Fitting the covariance data with one- and two-parameter exponential models, the correlation length, L_S, was determined to be 2.3 km by both covariance models.

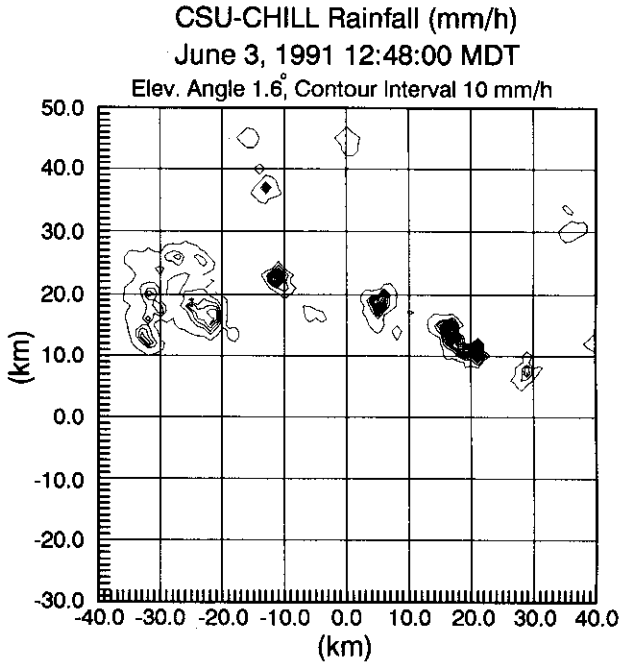

Fig. 2. Multi-parameter estimated rainfall at 12:48:00 MDT.

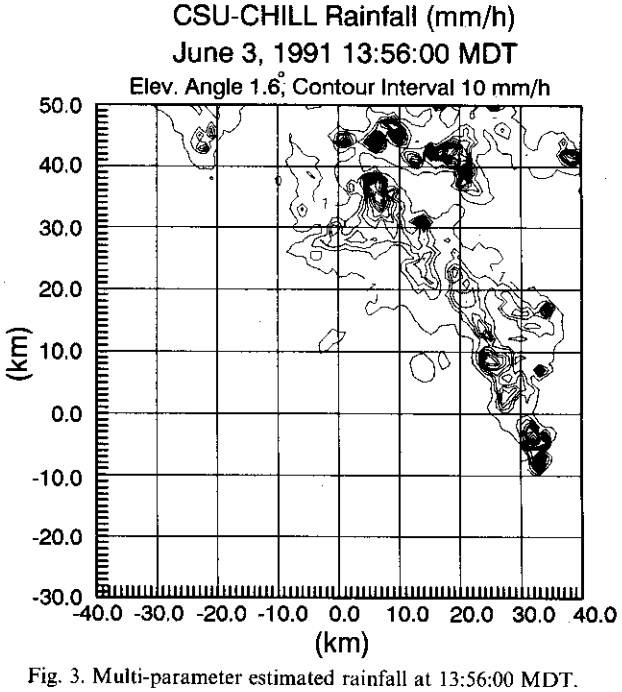

Fig. 3. Multi-parameter estimated rainfall at 13:56:00 MDT.

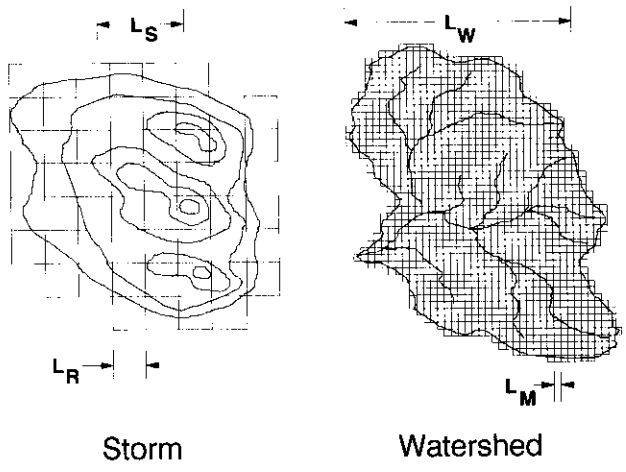

Fig. 4. Definition sketch of relevant length parameters— L_S, L_R, L_W and L_M.

6. Radar data resolution and length scales

Several studies presented in the literature review examined the effect of radar-rainfall data resolution on distributed hydrologic models, without general consideration of length scales. The discussion of length scales presented here represents a new development on this topic. Consider a convective rainstorm passing over a small (less than 150 km^2) watershed as shown in Fig. 4. There are five length parameters associated with this situation in the context of raster-based hydrologic models: the correlation length of the rainfall, L_S; the grid size of the rainfall data, L_R; the characteristic length of the watershed, L_W; the runoff model grid size, L_M; the correlation length of watershed characteristics. The radar and model resolution parameters L_R and L_M are defined by the modeler, whereas the basin and storm size parameters L_W and L_S are determined solely by the site and storm under study. In addition, it is important to note that the correlation length for watershed characteristics is of the order of tens to hundreds of meters, whereas the spatial correlation length for rainfall, L_S, is hundreds to thousands of meters.

There are three conditions which conceptually result in ideal physically based distributed hydrologic modeling. The first is $L_M \ll L_W$, so the basin is subdivided into sufficiently small grid elements to describe the spatial variability of basin characteristics. The second condition is $L_R \ll L_S$, which insures preservation of the spatial gradients of rainfall, particularly for smaller, convective rainstorms. The third requirement is that $L_R \leqslant L_M$, such that rainfall is placed in the correct watershed grid cell. The third strict requirement is most difficult to satisfy, as the practical minimum spatial resolution (approximately 1 km) of radar rainfall estimates cannot satisfy the third condition given the first.

The following analysis considers an ideal physically based hydrologic model, from which the deviations from ideal storm resolution and model input can be examined. Deviations from ideal modeling conditions are typically caused by input smearing,

which occurs as a result of spatial averaging over increasingly large areas. In this study, we focus on two distinct types of input smearing—storm smearing and watershed smearing.

Accepting that the third condition noted above must be relaxed, two surrogate parameters are used in substitution. The first parameter, L_R/L_S, describes storm smearing, and the second parameter, L_R/L_W, describes watershed smearing. Storm smearing occurs when the rainfall data length scale approaches or exceeds the rainfall correlation length, $L_R \rightarrow L_S$, which tends to decrease rain rates in high-intensity regions and increase rain rates adjacent in low-intensity regions, effectively reducing rain rate gradients. The reduction in rainfall intensity gradients owing to storm smearing is independent of basin size. Watershed smearing occurs when $L_R \rightarrow L_W$, and increases the uncertainty of the location of rainfall, which can result in the transfer of rainfall across basin boundaries. Watershed smearing is more likely to occur for smaller basins such as Macks Creek, at smaller values of L_R, than for larger basins such as Taylor Arroyo.

7. Radar resolution analysis

The effects of radar rainfall data grid size on surface runoff modeling for convective rainstorms on small watersheds (less than 150 km^2) are expected to result from storm smearing and watershed smearing. It is hypothesized that watershed smearing can be analyzed as a function of L_R/L_W describing the ratio of rainfall to basin length scales. As $L_R > L_S$ and $L_R \rightarrow L_W$, model error will have sources in both storm and watershed smearing.

The simulation method employed involves the transposition of radar rainfall data recorded in northern Colorado over two basins—one in southeastern Colorado, and one in southwestern Idaho. Given the large extent of the radar coverage (6400 km^2) compared with the areas of the two watersheds (e.g. 121 km^2 for the larger Taylor Arroyo), the precipitation field was subdivided into 50 independent subsets for Macks Creek and 40 independent subsets for Taylor Arroyo. Conceptually, a subset is a location for each basin within the large radar data domain as the storm evolves and passes over. Fig. 5 shows the locations within the 80 km × 80 km radar data domain where Macks Creek was positioned. Each location of Macks Creek in Fig. 5 is separated by a minimum distance of 4 km, which is greater than the correlation length L_S of the rainstorm, insuring reasonable independence between adjacent simulations. The rainfall fields are aggregated from the finest resolution by arithmetically averaging the data into larger grid cells.

The results from simulations with the finest resolution (L_R = 1 km) are the best available outflow calculations, and are used as reference outflow hydrographs. First, the results from all simulations with the tested input data resolutions: L_R = 2, 3, 4, 6, and 8 km, at one particular watershed location j, are normalized by the corresponding outflow variable obtained with rainfall data for the smallest grid size (1 km). The normalized peak discharge for any rainfall data grid size L_R and simulation j is denoted as $Q_p^*(L_R, j)$, and is calculated using the equation

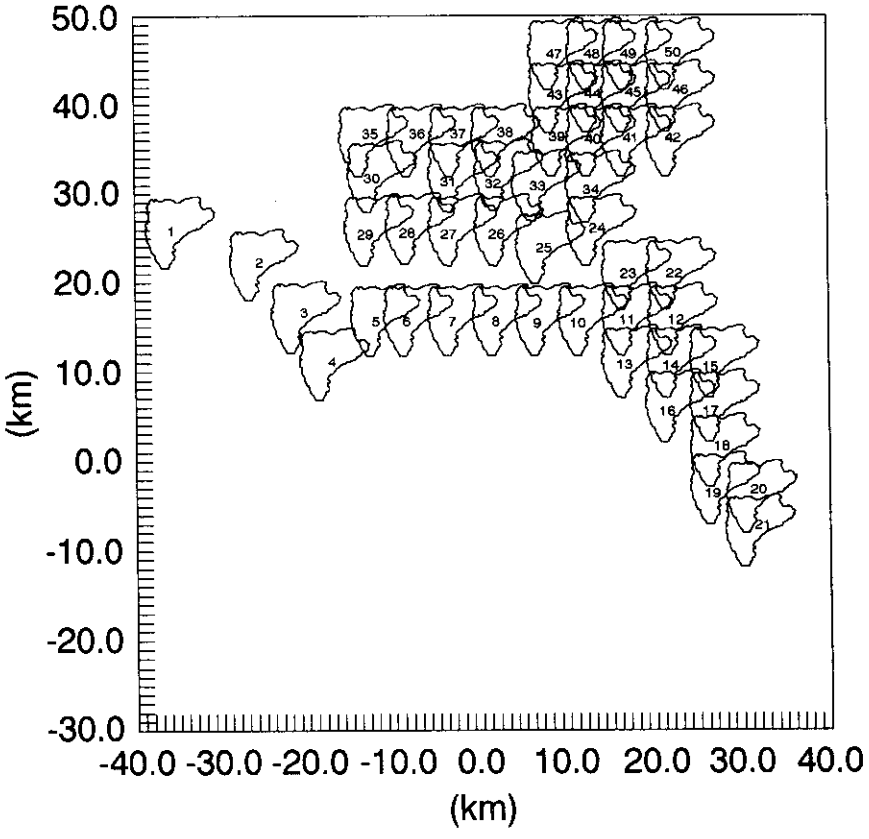

Fig. 5. Macks Creek test locations within the radar data domain.

$$Q_p^*(L_R,j) = \frac{Q_p(L_R,j)}{Q_p(1,j)} \tag{1}$$

Similarly, the normalized outflow and rainfall volumes for the jth simulation are calculated with

$$V_o^*(L_R,j) = \frac{V_o(L_R,j)}{V_o(1,j)} \tag{2}$$

and

$$V_r^*(L_R,j) = \frac{V_r(L_R,j)}{V_r(1,j)} \tag{3}$$

The mean normalized peak discharge, runoff volume, and rainfall volume over N simulations, where N is 50 for Macks Creek and 40 for Taylor Arroyo, are calculated

using

$$\bar{Q}_p(L_R) = \frac{1}{N}\sum_{j=1}^{N} Q_p^*(L_R,j) \tag{4}$$

$$\bar{V}_o(L_R) = \frac{1}{N}\sum_{j=1}^{N} V_o^*(L_R,j) \tag{5}$$

and

$$\bar{V}_r(L_R) = \frac{1}{N}\sum_{j=1}^{N} V_r^*(L_R,j) \tag{6}$$

The standard deviation of the normalized outflow variables for each tested L_R are determined using the following equations for the peak discharge, runoff volume and rainfall volume, respectively:

$$S_{Q_p}(L_R) = \left\{\frac{1}{N-1}\sum_{j=1}^{N}[\bar{Q}_p(L_R) - Q_p^*(L_R,j)]^2\right\}^{1/2} \tag{7}$$

$$S_{V_o}(L_R) = \left\{\frac{1}{N-1}\sum_{j=1}^{N}[\bar{V}_o(L_R) - V_o^*(L_R,j)]^2\right\}^{1/2} \tag{8}$$

$$S_{V_r}(L_R) = \left\{\frac{1}{N-1}\sum_{j=1}^{N}[\bar{V}_r(L_R) - V_r^*(L_R,j)]^2\right\}^{1/2} \tag{9}$$

This analysis technique produces one mean normalized outflow variable on Macks Creek and Taylor Arroyo, respectively, for each L_R tested over N simulations. The mean and standard deviation of these normalized outflow variables are used to identify trends and variability in the normalized outflow characteristics as a function of radar data resolution.

The effect of rainfall rate changes on surface runoff are examined for two types of simulations: (1) impervious basins for which the surface runoff volume will be maintained despite rain rate reductions in high-intensity regions; (2) pervious basins for which the surface runoff volume will decrease as a result of increased infiltration volume from reduced high-intensity rainfall regions.

8. Results without infiltration

The CASC2D outflow summary data for simulations without infiltration are used in the analysis. The rainfall volume is the primary indicator of watershed smearing. The mean $\bar{V}_r$ and standard deviation S_{V_r} of the normalized rainfall volume vs. the watershed smearing parameter L_R/L_W for both Macks Creek and Taylor Arroyo, are plotted in Fig. 6. There is little change in the storm total rainfall volume for

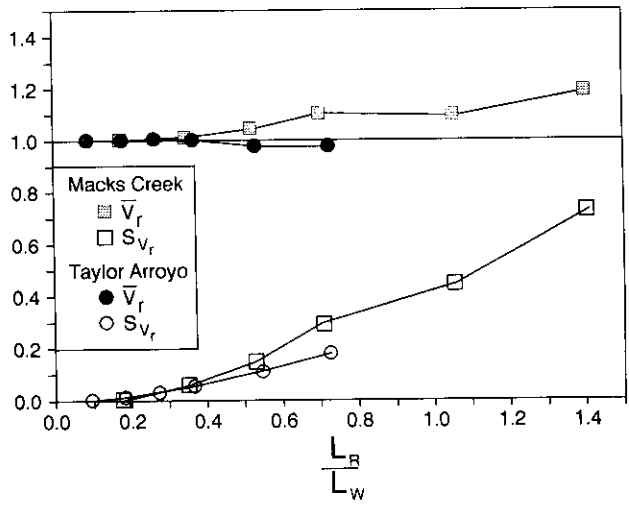

Fig. 6. Watershed smearing effect on rainfall volume for 50 storms on Macks Creek and 40 storms on Taylor Arroyo, without infiltration.

$L_R/L_W < 0.4$ for both basins. As L_R/L_W increases beyond 0.4, there is an increase in rainfall volume, V_r, for the smaller Macks Creek, and a decrease in V_r for Taylor Arroyo. The increase in the mean storm rainfall is larger for Macks Creek than the decrease observed for Taylor Arroyo. The standard deviation of normalized rainfall volume is also appreciably higher for the smaller Macks Creek basin.

It is impossible to separate the effects of watershed smearing and storm smearing in this analysis of the outflow variables because as $L_R \rightarrow L_S$ (storm smearing), L_R also approaches L_W (watershed smearing) for these small basins. However, storm smearing should occur first because $L_S < L_W$ for both basins. The relative magnitudes of the separate effects of input and storm smearing can be judged by comparing the deviation of the normalized outflow variables with decreasing resolution to the corresponding changes in rainfall volume. The mean, $\overline{Q}_p$, and standard deviation, S_{Q_p}, of the normalized peak discharge vs. the storm smearing parameter L_R/L_S for both watersheds are plotted in Fig. 7. The mean and standard deviation of the normalized outflow volume, $\overline{V}_o$, is similarly plotted in Fig. 8. Figs. 7 and 8 show a deviation in the normalized outflow variables $\overline{Q}_p$ and $\overline{V}_o$ from the simulations with the finest resolution, at the first level of aggregation, $L_R = 2$ km. The deviation of the normalized $\overline{Q}_p$ and $\overline{V}_o$ values from those in the simulations with the finest resolution is initially small. The rate of deviation increases is more substantial for both $\overline{Q}_p$ and $\overline{V}_o$ at values of L_R/L_S greater than 0.8 and 1.7 on Macks Creek and Taylor Arroyo, respectively. These L_R/L_S values correspond to $L_R/L_W = 0.4$ on both watersheds, indicating that watershed smearing is beginning to occur. The initial slight deviation of the normalized $\overline{Q}_p$ and $\overline{V}_o$ variables are caused by storm smearing as $L_R \rightarrow L_S$. However, as $L_R \rightarrow L_W$, watershed smearing begins, causing a substantial deviation of both $\overline{Q}_p$ and $\overline{V}_o$ with rainfall data aggregation.

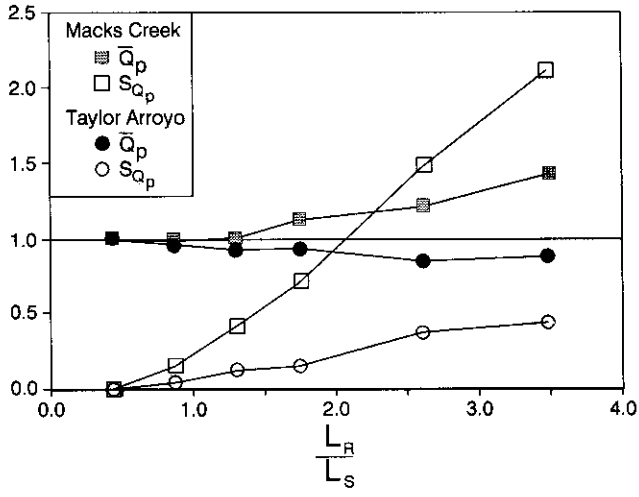

Fig. 7. Combined watershed and storm smearing effects on peak discharge for 50 storms on Macks Creek and 40 storms on Taylor Arroyo, without infiltration.

9. Results with infiltration

The procedures without infiltration detailed in the previous section are duplicated in these simulations. The only additional consideration is the effect of infiltration. The same rainfall data subsets as described previously are used in these simulations. Values of soil moisture deficit, M_d, tested on both watersheds, are 0.3, 0.1, and 0.0,

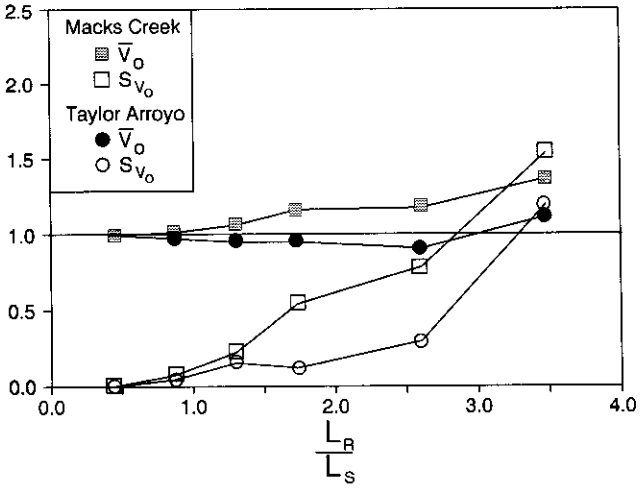

Fig. 8. Combined watershed and storm smearing effects on runoff volume for 50 storms on Macks Creek and 40 storms on Taylor Arroyo, without infiltration.

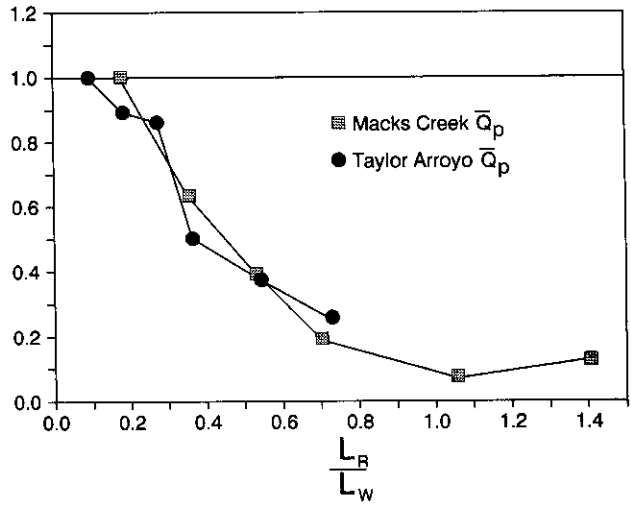

Fig. 9. Combined watershed and storm smearing effects on peak discharge for 11 storms on Macks Creek and 18 storms on Taylor Arroyo, with infiltration and $M_d = 0.3$.

corresponding to dry, wet, and saturated soil initial conditions, respectively. The selected M_d value is applied over the entire basin on all soil types.

The probability of a given storm producing runoff is less than 100% with infiltration, as opposed to the impervious case where every storm produces runoff. With the initial soil moisture deficit of 0.3 (dry conditions), only 11 and 18 rainfall data subsets generate runoff on Macks Creek and Taylor Arroyo watersheds, respectively. The analysis is performed only for rainfall data subsets which produce runoff. The peak discharge data vs. L_R/L_W for these simulations with runoff are plotted in Fig. 9. The mean normalized peak discharge for both watersheds decreases considerably as the rainfall data grid size increases. The watershed smearing parameter L_R/L_W produces reasonable agreement between the behavior of the two pervious basins to rainfall spatial aggregation.

The extreme reduction in peak discharge observed on both watersheds with increasing L_R/L_W indicates a decrease in the volume of excess rainfall, owing solely to rainfall data aggregation. The mean percentage of rainfall infiltrating for storms which produce runoff, versus L_R/L_W at initial soil moisture deficits of 0.3, 0.1, and 0.0 on both watersheds, is plotted in Fig. 10.

10. Conclusions

Two dimensionless similarity parameters which describe different aspects of the relationship between rainfall data spatial aggregation and distributed hydrologic model response are identified. The storm smearing parameter, L_R/L_S, describes a reduction in rain rate gradients. The watershed smearing parameter, L_R/L_W,

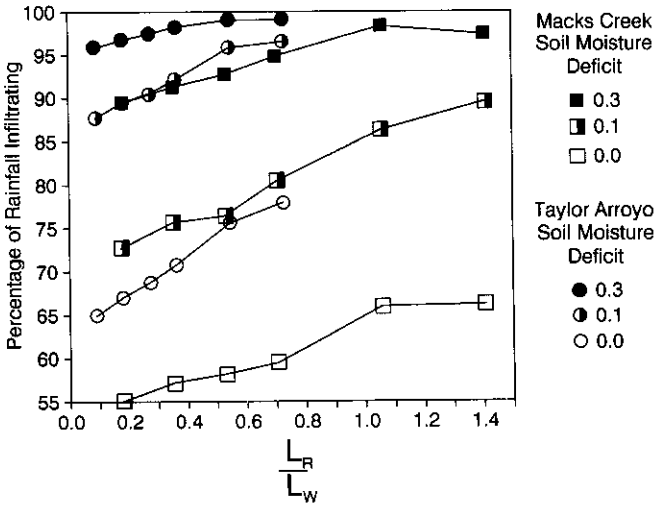

Fig. 10. Combined watershed and storm smearing effects on the percentage of rainfall infiltrating on Macks Creek and Taylor Arroyo for three values of M_d.

describes the uncertainty of rainfall location with respect to the watershed boundary. Simulations without infiltration reveal that watershed smearing is an important source of hydrologic model error when $L_R/L_W > 0.4$, owing to the change in basin-wide storm total rainfall volume, as shown in Fig. 6. The influences of storm smearing and watershed smearing are combined in the outflow variables Q_p and V_o for $L_R/L_W > 0.4$. Deviations of hydrologic model response from the finest-resolution results for $L_R/L_W < 0.4$ are caused primarily by storm smearing. The data in Figs. 7 and 8 indicate that watershed smearing is the main source of hydrologic model error on small catchments (less than 150 km^2).

Simulations with Green and Ampt infiltration reveal that the watershed smearing parameter L_R/L_W adequately describes the reduction of peak outflow owing to rainfall data aggregation as shown in Fig. 9. Significant reductions in $\overline{Q}_p$ with increasing L_R/L_W are caused by reduced excess rainfall rates as shown in Fig. 10. There is no evidence that the percentage of rainfall volume infiltrating converges as the rainfall data grid size is decreased. If the radar data are gridded at an artificially fine resolution ($L_R \leqslant L_M$), convergence must be observed. However, practical radar resolutions provide no convergence. These findings have several ramifications for the practical coupling of weather radar estimated rainfall rates and two-dimensional distributed parameter runoff models.

11. Acknowledgments

This work was performed at Colorado State University and funded by the US Army Research Office (Grant ARO/DAAL 03-86-0175). We acknowledge the

assistance of Dr. Bahram Saghafian and Dr. William Doe III with the watershed model and watershed data. Professor V.N. Bringi of the Department of Electrical Engineering, and Professor Steven Rutledge of the Department of Atmospheric Science, both at Colorado State University, provided access to the CSU-CHILL weather radar data. Special thanks are due to Dr. Walter Bach for his support of this effort. The constructive comments of three anonymous reviewers are also acknowledged and appreciated.

12. References

Austin, P.M., 1987. Relation between measured radar reflectivity and surface rainfall. Mon. Weather Rev., 115: 1053–1070.

Cabral, M.C., Bras, R.L., Tarboton, D. and Entekhabi, D., 1990. A distributed, physically based rainfall–runoff model incorporating topography for real-time flood forecasting. Ralph M. Parsons Laboratory, Rep. 332, Massachusetts Institute of Technology, Cambridge, MA, 220 pp.

Chandrasekar, V., Bringi, V.N., Balakrishnan, N. and Zrnic, D.S., 1990. Error structure of multiparameter radar and surface measurements of rainfall. Part III: Specific differential phase. J. Atmos. Oceanic Technol., 7(5): 621–629.

Chandrasekar, V., Gorgucci, E. and Scarchilli, G., 1993. Optimization of multiparameter radar estimates of rainfall. J. Appl. Meteorol., 32(7): 1288–1293.

Doe, III, W.W., 1992. Simulation of the spatial and temporal effects of Army maneuvers on watershed response. Ph.D. Dissertation, Department of Civil Engineering, Colorado State University, Fort Collins, 301 pp.

Green, W.H. and Ampt, G.A., 1911. Studies on soil physics, 1. The flow of air and water through soils. J. Agric. Sci., 4: 1–24.

Jameson, A.R., 1991. A comparison of microwave techniques for measuring rainfall. J. Appl. Meteorol., 30: 32–54.

Julien, P.Y. and Saghafian, B., 1991. CASC2D users manual—a two-dimensional watershed rainfall–runoff model. Civil Engineering Rep. CER90-91PYJ-BS-12, Colorado State University, Fort Collins, 66 pp.

Klazura, G.E. and Imy, D.A., 1993. A description of the initial set of analysis products available from the NEXRAD WSR-88D system. Bull. Am. Meteorol. Soc., 74(7): 1293–1311.

Kouwen, N., 1986. SIMPLE—a watershed model for flood forecasting. Users Manual. Department of Civil Engineering, University of Waterloo, Waterloo, Ont., 130 pp.

Kouwen, N. and Garland, G., 1989. Resolution considerations in using radar rainfall data for flood forecasting. Can. J. Civ. Eng., 16: 279–289.

Krajewski, W.F., Lakshmi, V., Georgakakos, K.P. and Jain, S.C., 1991. A Monte Carlo study of rainfall sampling effect on a distributed catchment model. Water Resour. Res., 27(1): 119–128.

National Research Council, 1991. Opportunities in the Hydrologic Sciences. Committee on Opportunities in the Hydrologic Sciences, Water Science and Technology Board, Commission on Geosciences, Environment, and Resources, National Research Council, National Academy Press, Washington, DC, 337 pp.

Ogden, F.L. and Julien, P.Y., 1993. Runoff sensitivity to temporal and spatial rainfall variability at runoff plane and small basin scales. Water Resour. Res., 29(8): 2589–2597.

Ogden, F.L. and Turk, F.J., 1991. The applicability of weather radar to hydrologic modeling: radar resolution requirements and comparison with dense raingauge network data. Proc. 11th Annual AGU Hydrology Days, 2–4 April 1991, Colorado State University, Fort Collins, CO, Hydrology Days Publications, Fort Collins, CO, pp. 11–22.

Pessoa, M.L., Bras, R.L. and Williams, E.R., 1993. Use of weather radar for flood forecasting in the Sieve River basin: a sensitivity analysis. J. Appl. Meteorol., 32(3): 462–475.

Rawls, W.J., Brakensiek, D.L. and Miller, N., 1983. Green–Ampt infiltration parameters from soils data. J. Hydraul. Eng. Am. Soc. Civ. Eng., 109(1): 62–70.

Sachidananda, M. and Zrnic, D.S., 1986. Differential propagation phase shift and rainfall rate estimation. Radio Sci., 21: 235–247.

Saghafian, B., 1992. Hydrologic analysis of watershed response to spatially varied infiltration. Ph.D. Dissertation, Department of Civil Engineering, Colorado State University, Fort Collins, 215 pp.

Seliga, T.A. and Bringi, V.N., 1976. Potential use of radar differential reflectivity measurements at orthogonal polarizations for measuring precipitation. J. Appl. Meteorol., 15: 69–76.

Seliga, T.A., Aron, G., Aydin, K. and White, E., 1991. Storm runoff simulation using radar-estimated rainfall rates and a unit hydrograph model (Syn-Hyd) applied to the Greve watershed. Proc. 25th Conf. on Radar Meteorol., Am. Meteorol. Soc., Paris, 1991, Am. Meteor. Soc., Boston, MA, pp. 587–590.